Data-point-wise spatiotemporal mapping of human ventral visual areas: Use of spatial frequency/luminance-modulated chromatic faces

竹田, 昂典

NeuroImage 239 (2021) 118325

Contents lists available at ScienceDirect

NeuroImage

journal homepage: www.elsevier.com/locate/neuroimage

Data-point-wise spatiotemporal mapping of human ventral visual areas: Use of spatial frequency/luminance-modulated chromatic faces

Akinori Takeda[a,b,*], Emi Yamada[a,c], Taira Uehara[a,d], Katsuya Ogata[a,e], Tsuyoshi Okamoto[f,g], Shozo Tobimatsu[a,h]

[a] Department of Clinical Neurophysiology, Neurological Institute, Faculty of Medicine, Graduate School of Medical Sciences, Kyushu University, 3-1-1 Maidashi, Higashi-ku, Fukuoka 812-8582, Japan
[b] Research Center for Brain Communication, Research Institute, Kochi University of Technology, 185 Miyanokuchi, Tosayamada, Kami City, Kochi 782-8502, Japan
[c] Department of Linguistics, Faculty of Humanities, Kyushu University, 744 Motooka, Nishi-ku, Fukuoka 819-0395, Japan
[d] Department of Neurology, IUHW Narita Hospital, 852 Hatakeda, Narita, Chiba 286-8520, Japan
[e] Department of Pharmaceutical Sciences, School of Pharmacy at Fukuoka, International University of Health and Welfare, 137-1 Enokidu, Okawa, Fukuoka 831-8501, Japan
[f] Faculty of Arts and Science, Kyushu University, 744 Motooka, Nishi-ku, Fukuoka 819-0395, Japan
[g] Graduate School of Systems Life Sciences, Kyushu University, 744 Motooka, Nishi-ku, Fukuoka 819-0395, Japan
[h] Department of Orthoptics, Faculty of Medicine, Fukuoka International University of Health and Welfare, 3-6-40 Momochihama, Sawara-ku, Fukuoka 814-0001, Japan

ARTICLE INFO

Keywords:
Magnetoencephalography
M170
Spatial frequency
Luminance
Facial color
Threshold-free cluster enhancement

ABSTRACT

Visual information involving facial identity and expression is crucial for social communication. Although the influence of facial features such as spatial frequency (SF) and luminance on face processing in visual areas has been studied extensively using grayscale stimuli, the combined effects of other features in this process have not been characterized. To determine the combined effects of different SFs and color, we created chromatic stimuli with low, high or no SF components, which bring distinct SF and color information into the ventral stream simultaneously. To obtain neural activity data with high spatiotemporal resolution we recorded face-selective responses (M170) using magnetoencephalography. We used a permutation test procedure with threshold-free cluster enhancement to assess statistical significance while resolving problems related to multiple comparisons and arbitrariness found in traditional statistical methods. We found that time windows with statistically significant threshold levels were distributed differently among the stimulus conditions. Face stimuli containing any SF components evoked M170 in the fusiform gyrus (FG), whereas a significant emotional effect on M170 was only observed with the original images. Low SF faces elicited larger activation of the FG and the inferior occipital gyrus than the original images, suggesting an interaction between low and high SF information processing. Interestingly, chromatic face stimuli without SF first activated color-selective regions and then the FG, indicating that facial color was processed according to a hierarchy in the ventral stream. These findings suggest complex effects of SFs in the presence of color information, reflected in M170, and unveil the detailed spatiotemporal dynamics of face processing in the human brain.

Abbreviations: ANOVA, analysis of variance; BEM, boundary element method; BSF, broadband spatial frequency; cpd, cycles per degree; cpi, cycles per image; dSPM, dynamic statistical parametric mapping; EEG, electroencephalography; EQU, equiluminant; ERF, event-related magnetic fields; FDR, false discovery rate; FG, fusiform gyrus; fMRI, functional magnetic resonance imaging; HPI, head position indicator; HSF, high spatial frequency; ICA, independent component analysis; IOG, inferior occipital gyrus; ISI, inter-stimulus interval; LGN, lateral geniculate nucleus; LSF, low spatial frequency; MCP, multiple comparisons problem; MEG, magnetoencephalography; MRI, magnetic resonance imaging; OFA, occipital face area; OTP, oversampled temporal projection; PPA, parahippocampal place area; ROIs, regions of interest; SD, standard deviation; SF, spatial frequency; TFCE, threshold-free cluster enhancement; tSSS, spatiotemporal signal space separation; V1, primary visual cortex.

* Corresponding author at: Department of Clinical Neurophysiology, Neurological Institute, Faculty of Medicine, Graduate School of Medical Sciences, Kyushu University, 3-1-1 Maidashi, Higashi-ku, Fukuoka 812-8582, Japan; Research Center for Brain Communication, Research Institute, Kochi University of Technology, 185 Miyanokuchi, Tosayamada, Kami City, Kochi 782-8502, Japan.
E-mail address: takinori@med.kyushu-u.ac.jp (A. Takeda).

https://doi.org/10.1016/j.neuroimage.2021.118325.
Received 11 November 2020; Received in revised form 4 June 2021; Accepted 29 June 2021
Available online 30 June 2021.

1. Introduction

Visual information is a fundamental resource for recognizing the natural environment, and supports essential non-verbal social communication such as face recognition. Color and spatial frequency (SF)/luminance are low-level features of visual input such as face images. This information is conveyed to the primary visual cortex (V1) via the lateral geniculate nucleus (LGN) and is then processed in parallel (Livingstone and Hubel, 1988; Tobimatsu and Celesia, 2006). The V1 receives inputs via two main pathways originating in the LGN—the pathway derived from the magnocellular (M) layers of LGN, which sends coarse SF information, and that from the parvocellular (P) layer, which sends color and fine SF information (Livingstone and Hubel, 1988). This structural visual information is then sent to a ventral visual stream (Merigan and Maunsell, 1993), where information related to color as well as low and high SF (LSF and HSF, respectively) is integrated. Importantly, the ventral stream contains specialized brain regions that process distinct aspects of visual images. For example, previous functional magnetic resonance imaging (fMRI) studies have identified V4 (McKeefry and Zeki, 1997) and V8 (Hadjikhani et al., 1998) as color-selective regions. Other ventral areas represent category selectivity. For instance, regions within the fusiform gyrus (FG) exhibit selective activation to faces (Grill-Spector et al., 2018; Kanwisher et al., 1997; Weiner and Grill-Spector, 2010), and a more medially located region called the parahippocampal place area (PPA) preferentially responds to scenes (Epstein and Kanwisher, 1998). Face-selective regions also exhibit a preference for LSF information in visual stimuli (Canário et al., 2016; Woodhead et al., 2011), whereas the PPA responds more strongly to HSF information (Rajimehr et al., 2011). Electrophysiological studies have identified a face-selective component called the N170 (Bentin et al., 1996). This and its magnetic counterpart, M170 (Liu et al., 2000, 2002), are considered to originate from the FG (Deffke et al., 2007; Halgren et al., 2000; Perry and Singh, 2014; Pourtois et al., 2010). SF information has been found to significantly affect these components (Awasthi et al., 2013; Goffaux et al., 2003; Hsiao et al., 2005; Jeantet et al., 2019; McFadyen et al., 2017; Nakashima et al., 2008).

Researchers have developed various visual stimuli to study the influence of low-level visual features on face processing in the ventral visual areas. Most previous studies have used grayscale stimuli with isolated SF components (Awasthi et al., 2013; Eger et al., 2004; Goffaux et al., 2003, 2011; Hsiao et al., 2005; Iidaka et al., 2004; Jeantet et al., 2018, 2019; McFadyen et al., 2017; Méndez-Bértolo et al., 2016; Morrison and Schyns, 2001; Nakashima et al., 2008; Pourtois et al., 2010; Vuilleumier et al., 2003), and some researchers further developed hybrid images containing both LSF and HSF components in different categories (Rotshtein et al., 2007, 2010; Winston et al., 2003). Chromatic face stimuli containing only color information have also been used in some face studies (Cushing et al., 2019; Im et al., 2017; Nakashima et al., 2008). These have no SF information because the luminance values of all pixels within the stimulus are equal, and therefore, these equiluminant (EQU) chromatic stimuli can input color information to the P pathway exclusively. However, to the best of our knowledge, face stimuli containing both color and modified SF information have not been created. Thus, the ways in which simultaneously received color and selected SF information affect the responses in the ventral areas remains unknown. To elucidate this in the present study, we developed a digital image processing method to enable modulation of SF components in natural and complex chromatic pictures while preserving color information, and created chromatic stimuli containing LSF or HSF components (chromatic LSF and HSF stimuli) and EQU chromatic stimuli (Fig. 1A). Chromatic LSF images are expected to input low SF information to the M pathway and color information to the P pathway. In contrast, chromatic HSF images are expected to simultaneously input high SF and color information to the P pathway. Hence, using these stimuli in addition to the original chromatic images, which contain broadband SF (BSF) information, enables concurrent inputting of different SF and color information to the M and P pathways.

Characterizing the spatiotemporal dynamics of specific cortical areas represents an important but challenging objective. Non-invasive techniques such as MRI, fMRI, and diffusion-weighted imaging have vastly enriched our understanding of the structure and localized function of the human brain (Amunts et al., 2014; Evans et al., 2012). However, brain atlases generated using these techniques are limited in terms of temporal information because of their relatively low temporal resolution. Magnetoencephalography (MEG) is a functional neuroimaging technique for detecting magnetic fields produced by electrical currents in the brain (Baillet, 2017; Hämäläinen et al., 1993; Tobimatsu and Kakigi, 2016). Because MEG has an excellent temporal resolution and a spatial resolution that is nearly equal to that of fMRI when using source reconstruction methods, many studies have applied MEG to cognitive brain processes with multiple sensory stimuli (Hari and Puce, 2017). However, further improvements to MEG data acquisition and analysis methods are needed to accurately map the detailed spatiotemporal dynamics of distinct brain areas.

One issue preventing detailed spatiotemporal mapping of brain activity is the multiple comparisons problem (MCP). The MCP is an issue that arises during statistical analysis of electroencephalography (EEG) and MEG data in which repeating a statistical test increases the probability that the null hypothesis will be falsely rejected (Maris, 2012). To address this, MEG researchers frequently adopt nonparametric permutation test procedures that involve clustering (Maris and Oostenveld, 2007). Specifically, spatiotemporally adjacent data points are regarded as clusters, and statistical significance is calculated for the clusters. However, an arbitrary threshold for cluster formation must be selected in addition to the one for significance inference (Maris and Oostenveld, 2007), and the choice of threshold can greatly affect the analysis results. To address this concern, we adopted a recently developed algorithm termed threshold-free cluster enhancement (TFCE; Smith and Nichols, 2009). Permutation tests with TFCE can successfully handle the MCP and do not require thresholds for initial cluster formation.

In this study, we systematically investigated the effects of different combinations of SF and color on M170 responses. Participants viewed chromatic images of faces and houses in four SF conditions, presented in a pseudo-random order during MEG recording. After converting obtained sensor M170 data to source waveforms with fine spatiotemporal resolution, a nonparametric test procedure with TFCE was applied to the source data to map the spatiotemporal modulations of M170 responses. Statistical inference was carried out in accordance with the standard two-way analysis of variance (ANOVA) procedure (Figs. 2D and S4). We had two main research goals. The first was to characterize the spatiotemporal dynamics of the human ventral visual areas related to the processing of color and SF of faces, and the second was to map the functional hierarchy within these regions in more detail.

2. Materials and methods

2.1. Participants

Eighteen healthy adults (9 women, 21–41 years old) with normal or corrected-to-normal visual acuity participated in this study. We confirmed all participants to be right-handed with normal color vision, as assessed using the Edingbach Handedness Inventory (Oldfield, 1971) and Ishihara color plate test (Handaya Co., Ltd., Tokyo, Japan), respectively. Written informed consent was obtained from all participants prior to commencing the experiment. The present study was carried out in accordance with the Declaration of Helsinki, and approved by the Ethics Committee of the Graduate School of Medical Sciences, Kyushu University.

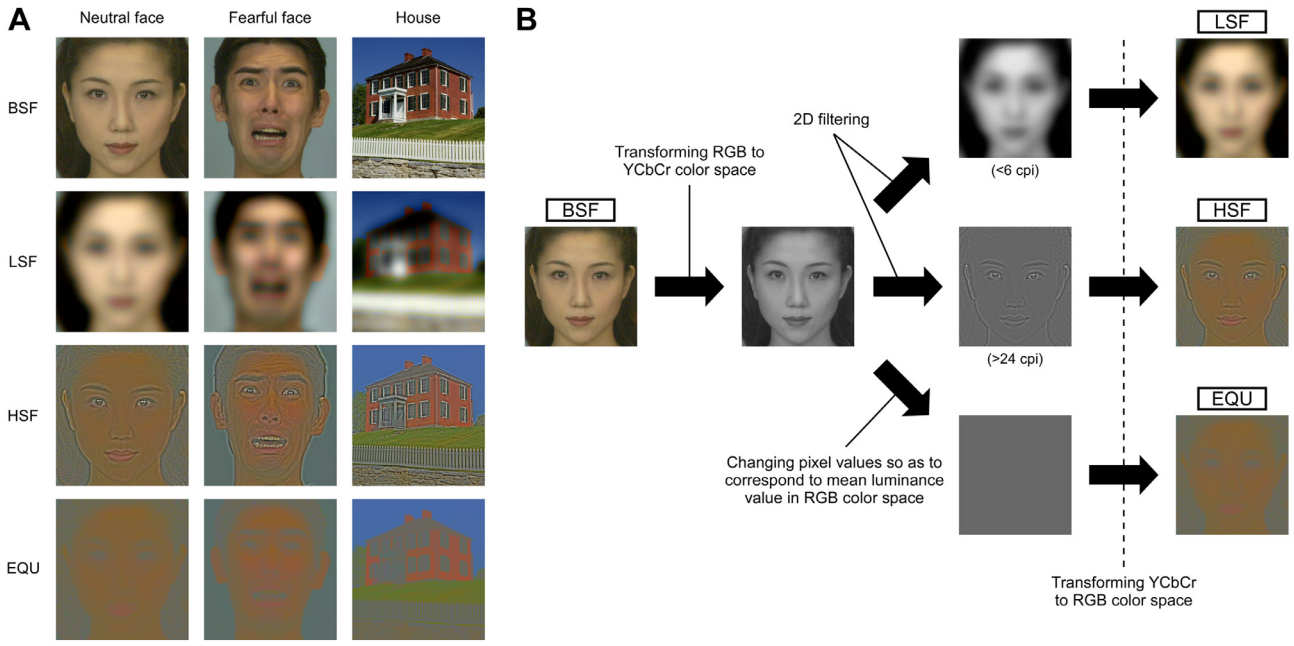

Fig. 1. Visual stimuli. **(A)** Examples of chromatic BSF, LSF, HSF, and EQU images of faces with neutral and fearful facial expressions and a house. The chromatic BSF images contain all of the physical features of the faces and house, and theoretically activate both the magnocellular (M) and parvocellular (P) pathways. The chromatic LSF images input low SF information to the M system and color information to the P system. The chromatic HSF images input high SF information and color information into the P pathway simultaneously. Because chromatic EQU images have only color information, the P system is activated but the M system is silenced. **(B)** Image processing flow of chromatic spatially-filtered and EQU stimuli. The chromatic LSF, HSF, and EQU stimuli were created from the original BSF images via transformation between the RGB and YCbCr color spaces. We used a transformation to the YCbCr color space because it contains luminance and color information as independent axes, which allows us to modify the intensity while retaining color information. For the chromatic LSF and HSF stimuli, after BSF images were transformed from RGB to YCbCr color space, the luminance dimension (Y axis in YCbCr color space) was spatially filtered using a second-order Butterworth filter. After adjustments to the mean luminance, filtered YCbCr images were transformed back to RGB color space. For EQU images, the values of pixels in the luminance dimension of YCbCr color space were modified so that all pixel values in the resulting RGB images were in accordance with the mean luminance value across the original images. After this adjustment, the YCbCr images were converted back to RGB color space. Abbreviations: BSF, broadband spatial frequency; LSF, low spatial frequency; HSF, high spatial frequency; EQU, equiluminant.

2.2. Visual stimuli

We used three types of visual images: neutral faces, fearful faces, and houses (Fig. 1A). Chromatic neutral and fearful face images were obtained from the ATR database (ATR-Promotions Inc., Kyoto, Japan), and six house images were obtained from a website that provided free color pictures. We also used nine food pictures from the International Affective Picture System (Lang et al., 2008) as targets in the experimental task. Detailed image information is provided in Table S1.

We adopted transformation between RGB and YCbCr color space to adjust the mean luminance of images and to create spatially filtered and EQU chromatic stimuli (Fig. 1B). YCbCr color space represents images according to a luminance component (Y) and blue- (Cb) and red-color-difference components (Cr). Therefore, transformation to the YCbCr color space allows us to modify the image luminance intensity independent of color information retained in the Cb and Cr components. Each component value in YCbCr color space was calculated using red (R), green (G), and blue (B) values in RGB color space according to the following equations:

$$Y = 0.299R + 0.587G + 0.114B,$$

$$Cb = -0.169R - 0.332G + 0.5B,$$

$$Cr = 0.5R - 0.419G - 0.081B.$$

In contrast, transformation from YCbCr to RGB color space was carried out as follows:

$$R = Y + 1.402Cr,$$

$$G = Y - 0.714Cr - 0.344Cb,$$

$$B = Y + 1.772Cb.$$

We used the *rgb2ycbcr* and *ycbcr2rgb* functions implemented in the Image Processing Toolbox in Matlab 7.5 (MathWorks Inc., Natick, MA).

For chromatic BSF stimuli, we adjusted the mean luminance values using the RGB-YCbCr transformation. The original chromatic images of faces, houses, and foods were first cropped into a rectangular shape (320 × 340 pixels). The cropped images were converted from RGB to YCbCr color space, and the mean pixel values on the luminance axis (Y component) of the individual images were equalized to the mean Y-value across all BSF images of faces, houses, and foods (mean Y-value = 105, value range = 16–235; this resulted in a luminance value of 104 from 256 grayscale levels) using the SHINE toolbox (Willenbockel et al., 2010). The processed YCbCr images were transformed back to RGB color space, and we used the resultant face and house images as chromatic BSF stimuli and the food images as targets in a task conducted during MEG recording.

We also created chromatic LSF and HSF stimuli using the RGB-YCbCr color space transformation. Rectangular RGB face and house images with margins of 16 pixels on each side were transformed to YCbCr images, and a two-dimensional second-order Butterworth filter was then applied to the luminance axes. We used rectangular images with margins because spatial filtering yielded unnatural higher or lower luminance values at the fringe areas of the images. Cut-off values of < 6 cycles per image (cpi) and > 24 cpi were used for LSF and HSF stimuli, respectively. We adopted the same cut-off values used in previous studies

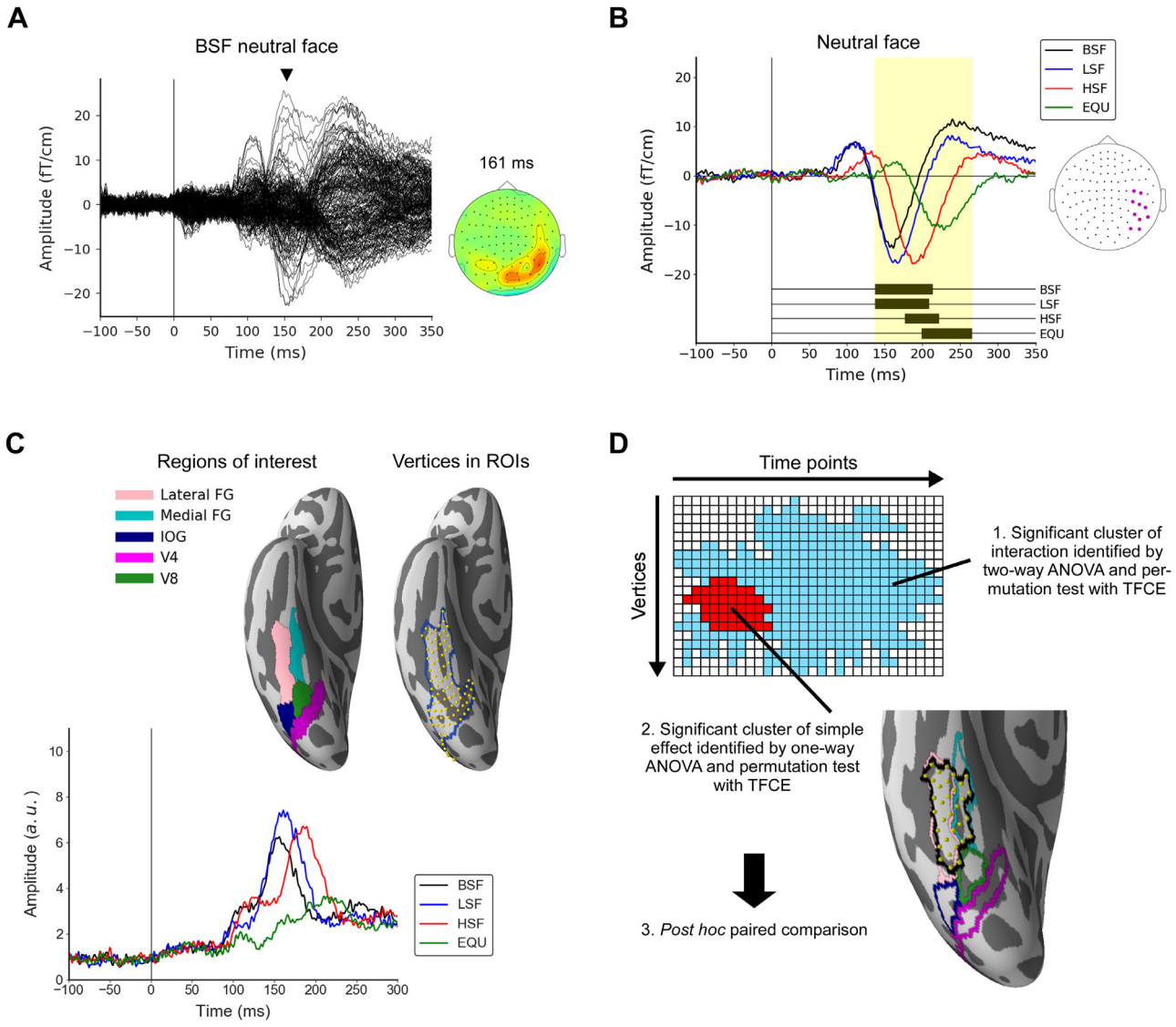

Fig. 2. Analytical procedures. **(A)** Sensor ERF waveforms. We observed face-selective activities (M170) in response to face stimuli in the occipitotemporal sensors (black arrow head). **(B)** Time windows of the M170 and mean ERF waveforms across the MEG sensors. The time windows (left, black squares) and sensors (right, magenta circles) were identified by a within-trial (*i.e.* pre- vs. post-stimulus) comparison approach combined with a nonparametric permutation test procedure with TFCE. The mean peak latencies of the M170 elicited by the neutral face varied depending on the SF condition. We adopted a time window of 137–265 ms (yellow shaded area) in the following statistical analysis. **(C)** Reconstructed source waveforms and regions of interest (ROIs). Sensor waveforms were converted to source waveforms at vertices on the brain surface by dSPM (lower section). We analyzed 97 vertices within the ROIs in the subsequent statistical analysis (upper section). **(D)** Schematic workflow of the two-way ANOVA with the permutation test procedure and TFCE. We calculated test statistics for the interaction between stimulus category and SF, and simple effects at each factor level in the individual data points using a repeated-measures two-way ANOVA and subsequent one-way ANOVA, respectively. We resolved the MCP in each processing step and assessed statistical significance via a nonparametric permutation test procedure with TFCE. The significant data points formed spatiotemporal clusters of the interaction (blue) and simple effects (red). Finally, *post hoc* comparisons were carried out using the Wilcoxon signed-rank test. Abbreviations: ERF, event-related magnetic fields; MCP, multiple comparisons problem; TFCE, threshold-free cluster enhancement; dSPM, dynamic statistical parametric mapping; FG, fusiform gyrus; IOG, inferior occipital gyrus; ANOVA, analysis of variance; SF, spatial frequency.

(McFadyen et al., 2017; Méndez-Bértolo et al., 2016; Vuilleumier et al., 2003). After spatial filtering, we rescaled the range of luminance values in the areas without margins. This process is important because values outside this range would be converted to the highest or lowest values, making the resultant images look unnatural. The luminance values in YCbCr color space range from 16–235, unlike common grayscale, which has value range of 0–255. Therefore, we rescaled the luminance value distributions within the areas without margins by normalizing them in a range from 0–219 and subsequently adding a value of 16 to all pixels. After rescaling, the mean luminance values (excluding the margin area) were adjusted to the mean luminance values among the BSF and target stimuli using the SHINE toolbox. Finally, these YCbCr images were converted back to RGB color space, and the margin pixels were cropped out.

For images with a spatially-filtered SF distribution, visual angle is an important factor in addition to the filter cut-off values because it strongly affects whether the filtered images properly stimulate the target visual pathway. As previously discussed (Canário et al., 2016; Rotshtein et al., 2007, 2010), psychophysical evidence has indicated that the threshold of 1.5 cycles per degree of visual angle (cpd) may be helpful in determining which of the M and P systems is predominantly activated (Skottun, 2000). In the present study, visual stimuli were presented in the participants' central visual field with visual angles of $6.66^{\circ} \times 7.07^{\circ}$, which resulted in cut-off values of 0.90×0.85 cpd

for chromatic LSF stimuli and 3.60 × 3.39 cpd for chromatic HSF stimuli. Therefore, we assumed that our spatial filtering and stimulus presentation settings would remove almost all of the undesirable SF components of the images that would activate the non-target pathway and retain the components that would preferentially activate the target pathway (Fig. S1).

Similarly, EQU chromatic stimuli were created using the RGB-YCbCr color space transformation (Fig. 1B). The stimuli contained color information, but no specific SF information (only zero-frequency component) because all pixels had the same luminance value. We made the images by changing the pixel values in the luminance dimension so that all pixel values in the resultant RGB images corresponded to the mean luminance value among the chromatic BSF and target stimuli. We used the following iterative procedure:

(i) Chromatic BSF images were converted to YCbCr color space.
(ii) All pixel values in the luminance axis were equalized to the mean luminance value among the BSF and target stimuli in YCbCr color space. Information regarding the equalized pixel values in the luminance dimension was retained as template data.
(iii) The YCbCr images with modulated luminance axes were transformed back to RGB color space. We tested whether all pixel values were equal to the mean luminance value in the RGB color space by converting from RGB to grayscale images using the *rgb2gray* function in the Image Processing Toolbox.
(iv) If we identified pixels with luminance values that were not equal to the mean RGB luminance value, we weighted the luminance values of the corresponding pixels in the template data.
(v) The luminance components of the YCbCr images were exchanged for the weighted template. The modulated YCbCr images were then converted back to RGB color space and checked.
(vi) Processes (iv) and (v) were repeated until all of the pixel values were equal to the mean luminance value in the obtained RGB images.

Rather than simply replacing the luminance axis values to a target value, we adopted this iterative process because some pixels in the resultant RGB images had slightly different values from the target mean luminance value. This was likely due to the temporal conversion between integer and floating-point data used in our script, which was required for precise computation. For the majority of images used in the present study, the process converged after the second round of the iterative procedure.

The two-dimensional amplitude spectra for each SF stimulus condition are provided in Supplementary Materials (Supplementary Texts and Figs. S2 and S3).

2.3. Experimental design and procedure

During MEG recording, visual stimuli were presented for 300 ms on a 32-inch LCD monitor (Display++; Cambridge Research Systems Ltd., Rochester, UK) with a refresh rate of 120 Hz. The monitor was calibrated prior to the experiment and positioned 2.5 m from the participants. Stimuli were presented in pseudo-random order such that identical individual images with the same SF components were not presented in succession. This was because a previous fMRI study reported that the aforementioned repetitive presentation strongly suppressed activity in face-selective areas (Eger et al., 2004). The target food stimuli were presented for 300 ms in random order, and successive presentation was permitted. The inter-stimulus interval (ISI) varied randomly from 900 to 1100 ms, and a white cross (visual angle of 1°) was presented on the monitor during the ISI. In each block, individual neutral faces, fearful faces, and houses were presented once in each SF condition (72 individual stimuli in total), and the target was presented 24 times. One run consisted of two blocks with a brief rest interval of 8 s, and the target was displayed on the monitor for 6 s at the beginning of each run. Targets were identical through individual runs but not across runs. Participants were instructed to fixate on the cross, and to press the left or right button on a computer mouse using their right or left index finger, respectively, as quickly as possible when the target was presented. They were told prior to the trial block which button and index finger to use. The order of response sides was counterbalanced across subjects: nine participants (four men and five women) pressed the right button using their right index finger in the first block in each run, whereas the other participants pressed the left button using their left index finger in the first block. The response side alternated in each block. We carried out nine runs with rest periods between each run. Before the main MEG recording, we recorded magnetic field fluctuations in an empty room for 2 min. Then, we recorded neuromagnetic activities during a rest period in which the participants were asked to engage in gaze fixation for 3 min ("participant noise"). Following this, we conducted a short practice session to train the participants on the experimental task. The experimental flow and stimulus presentation were controlled using PsychoPy (Peirce, 2007; Peirce et al., 2019).

2.4. Data recording

Electromagnetic responses were recorded using a 306-channel whole-head MEG system (Neuromag; Elekta Ltd., Helsinki, Finland). All recordings were conducted in a dim magnetically shielded room with the participant sitting in an upright position. The sampling frequency was 1000 Hz, and the signals were filtered using an online 0.03–330 Hz band-pass filter. Before recording, four head position indicator (HPI) coils were attached to the participant's scalp. Then, three anatomical landmarks (nasion and bilateral preauricular points), HPI coil positions, and at least 200 head surface locations were measured using a 3D digitizer (Fastrak; Polhemus, Colchester, VT, USA). HPI measurements were conducted at the beginning of the participant noise recording and the individual main recording sessions, and participants were instructed to maintain their head position during these recordings. Electrooculography was also recorded using electrodes placed above and below the left eye and on the bilateral outer canthuses. MRI structural images were obtained using 3T MRI scanners: a MAGNETOM Spectra (Siemens, Erlangen, Germany) for three participants and an Achieva 3.0T TX (Philips N.V., Eindhoven, the Netherlands) for the others.

2.5. Sensor data processing

We used MNE-Python software (Gramfort et al., 2013; Jas et al., 2018) for the majority of the subsequent data processing. First, oversampled temporal projection (OTP) (Larson and Taulu, 2018) using this software and spatiotemporal signal space separation (tSSS) (Taulu and Simola, 2006) using Elekta MaxFilter software were conducted for the sensor data. We also used the MaxMove function in the tSSS process, and the head positions in the MEG data were converted to those in the participant noise recording. After applying a 1–200 Hz zero-phase finite impulse response band-pass filter and a 60 Hz notch filter to the processed data, we used independent component analysis (ICA) to remove artifact components such as blinks and cardiac activity. The denoised data were segmented into 1.5 s epochs (750 ms before and after stimuli onset), and ICA was again applied to remove rectangular-wave-shape components, which are considered to be artifacts derived from the presence of the monitor. We defined the following three types of trials as those in which the behavior did not conform to the expectations of the task (erroneous trials): (i) target trials where subjects used the wrong finger to press the button, (ii) target trials without a button press, and (iii) stimulus trials with a button press. After excluding them, the remaining trials were visually inspected, and noisy ones were excluded. We randomly extracted 100 trials from the residual trials for each of 12 stimulus categories × SF combinational conditions and conducted baseline correction using mean values from the pre-stimulus onset interval (−100 to 0 ms). Finally, sensor event-related magnetic field (ERF) waveforms were obtained by averaging across trials (Fig. 2A). Partici-

pant noise data were also processed by OTP, tSSS, band-pass and notch filters, and then ICA.

2.6. Reconstructing source waveforms

T1-weighted MRI structural images were processed using FreeSurfer (Fischl, 2012). We used MNE-C software (Gramfort et al., 2014) to calculate head models via the boundary element method (BEM) and to conduct MEG-MRI co-registration. We computed forward solutions using the three-shell BEM model (Stenroos et al., 2014). Using dynamic statistical parametric mapping (dSPM; depth weight: 0.8, loose orientation constraint: 0.2, signal-to-noise ratio: 3) (Dale et al., 2000), we reconstructed source waveforms in three orientations at each vertex on the cortical surface from sensor ERFs, and then combined them by taking the norms. Noise covariance data were obtained from the participant noise data using the shrunk covariance estimator (Engemann and Gramfort, 2015) with rank estimation and reduction. For group analysis, individual cortical surfaces were morphed to a standard surface model provided by FreeSurfer (fsaverage, derived from the MNI-305 template brain). We adopted the 6th order octahedron model of fsaverage (4098 vertices per hemisphere with 4.9 mm spacing) to reduce computational load. Although source estimation was performed with a whole brain model, we used source waveform data from the right hemisphere only in the group-level statistical analysis because we observed a clearer M170 in the right occipitotemporal sensors when defining the M170 time window. We further selected five region labels in the parcellation atlas of the Human Connectome Project (HCP-MMP1.0) (Glasser et al., 2016) as regions of interest (ROIs; Fig. 2C). In addition to labels for the lateral FG (labeled as “FFC” in the reference (Glasser et al., 2016)) and medial FG (“VVC”), we focused on the inferior occipital gyrus (IOG; “PIT”) because some studies (Henson et al., 2009; Itier et al., 2006; Jacques et al., 2019; Rossion et al., 2003) have indicated that this region contributes to the generation of N170/M170. Labels for V4 and V8 were also included. We analyzed a total of 97 vertices within these ROIs without averaging the waveforms across vertices.

2.7. Permutation test procedure with TFCE

We adopted a nonparametric permutation test procedure with TFCE to avoid arbitrary thresholding for cluster formation. Test statistics (t or F values) at each data point were first calculated, and TFCE (starting threshold: 0, step size: 0.2, height weighting parameter: 2, extent weighting parameter: 0.5) was then applied. The TFCE algorithm calculated weighted test statistics (TFCE scores) for individual data points based on the initial test statistics (Smith and Nichols, 2009), and retained the maximum score value. This process was repeated 1000 times with random shuffling of the condition labels, and the obtained maximum values composed a permutation null distribution. Finally, TFCE scores at all data points based on the original datasets were compared with the null distribution, and corresponding p values were calculated. This comparison with the null distribution composed of maximum TFCE scores in each permutation has been shown to enable resolution of the MCP (Smith and Nichols, 2009). Consequently, individual time points and sensors or vertices have their own TFCE scores and corresponding p values.

2.8. Defining the time window of the M170 component

Prior to statistical analyses of the MEG source data, we determined the temporal data range for the M170 responses. To achieve this, we used sensor ERF data of neutral face condition and a within-trial comparisons approach (Maris and Oostenveld, 2007) combined with the permutation test procedure with TFCE. We selected neutral face data because we expected it to reflect pure neural responses to faces without additional factors such as emotion. Pre- (−350 to 0 ms) and post-stimulus onset data (0 to 350 ms) were compared using a two-tailed paired t test (Maris and Oostenveld, 2007), and TFCE scores and corresponding p values were calculated using the aforementioned test procedure. Data points with p values that corresponded to the smallest threshold (that is, $p = 0.001$) were used to specify the narrow time window. We repeated the assessment for each SF condition for the neutral face and focused on the right occipitotemporal sensors commonly found across all SF conditions. We then determined the continuous time points around the negative peaks in the sensors as individual time windows during which the M170 emerged in each SF condition. We focused on occipitotemporal sensors and negative deflections because previous studies have found N170/M170 components in the occipitotemporal area (Bentin et al., 1996; Deffke et al., 2007; Goffaux et al., 2003; Hsiao et al., 2005; Jeantet et al., 2019; Liu et al., 2000, 2002; Nakashima et al., 2008; Prieto et al., 2011), and the M170 has been observed as an ERF component with a negative amplitude in Neuromag gradiometer data (Hsiao et al., 2005; McFadyen et al., 2017; Prieto et al., 2011). Finally, we determined the time range including all time windows in the four SF conditions as the general M170 time window (Fig. 2B yellow shaded area).

2.9. Statistical analysis of source data

Spatiotemporal differences among the stimulus conditions in the source data were first assessed via a repeated-measures two-way ANOVA. If a significant interaction was observed, a one-way ANOVA was carried out. These ANOVA processes were conducted with the abovementioned test procedure with TFCE, and the statistical significance level was set at $p < 0.05$. For the two-way ANOVA processing, we first obtained F statistics for the main effects of category type (neutral face, fearful face, and house) and SF condition (BSF, LSF, HSF, and EQU), and their interaction for each data point. Then, we calculated null distributions, TFCE scores, and corresponding p values. Subsequent one-way ANOVAs for simple effects at each category or SF level were conducted for the data points that showed significant interactions (blue area in Figs. 2D and S4). This processing enabled us to identify spatiotemporal clusters of data points that indicated significant simple effects (red area in Fig. 2D; see also Fig. S4). Given that MEG signals are considered to originate in spatiotemporally summated postsynaptic potentials (Baillet, 2017; Hämäläinen et al., 1993), which last for more than 10 ms, it is reasonable to consider source activities lasting only a few milliseconds or isolated vertices to be unnatural. Therefore, we analyzed only significant clusters that lasted more than 10 ms, and excluded isolated vertices. Finally, we conducted *post hoc* paired comparisons via the Wilcoxon signed-rank test for each simple effect using mean values within their significant clusters, and the multiple comparisons were corrected by controlling the false discovery rate (FDR) using the Benjamini–Hochberg procedure (Benjamini and Hochberg, 1995). The significance level was set to an FDR-corrected p value of 0.05.

Apart from the ANOVA approaches, we assessed source neuromagnetic activities elicited by the EQU stimuli. We used a within-trial comparison analysis together with the above-mentioned test procedure to establish the detailed spatiotemporal dynamics after stimulus onset within ROIs. We compared source data points in the 300 ms post-stimulus onset period with those in the 300 ms pre-stimulus baseline period using paired t tests. We assessed the statistical significance using the same method employed when defining the M170 time window. We adopted a rigorous significance level of 0.005 because we expected that a large number of data points would have relatively smaller p values due to the low amplitude and small variance of the pre-stimulus onset data.

3. Results

3.1. Task performance of participants

We calculated the rate of erroneous trials for all trials (error rate) and the time interval from target onset to the button press (reaction time)

for each participant after the erroneous trials were extracted. The mean error rate and standard deviation (SD) across participants was 1.34 ± 1.54%, and the mean reaction time and SD across participants was 447.7 ± 45.4 ms. The low error rate and fast reaction time verified that the participants performed the task with a high level of wakefulness.

3.2. Determining the temporal data range

We observed statistically significant differences in the negative deflections (M170 responses) compared with the baseline for the neutral face stimuli in all SF conditions (BSF: TFCE scores = 76.11–103.00, LSF: TFCE scores = 68.92–88.12, HSF: TFCE scores = 87.97–90.42, EQU: TFCE scores = 82.38–86.68, all $p = 0.001$; Fig. 2B). These differences were driven by different clusters of the right occipitotemporal sensors, across which 11 gradiometers at 10 sensor positions were typically included (Fig. S5A). Based on the time windows identified in each SF condition (BSF: 137–213 ms, LSF: 137–208 ms, HSF: 177–221 ms, EQU: 199–265 ms), we defined the time period from 137–265 ms as the time window for the M170 component (yellow shaded area in Fig. 2B). Thus, the time range of the source data was restricted to this M170 time window.

3.3. Main effects of category and SF, and their interaction

Using the two-way ANOVA approach combined with the permutation test procedure and TFCE, we found a significant main effect of category, which corresponded to two independent clusters exhibiting distinct spatiotemporal profiles. The first cluster was observed in the lateral and medial FG at 158–206 ms (TFCE scores = 60.65–92.90, $p = 0.005$–0.049), whereas at 204–265 ms, the second one first appeared in the IOG and V4, and then extended over all ROIs (TFCE scores = 60.80–108.59, $p = 0.002$–0.049). We also observed a significant cluster compatible with the main effect of SF (TFCE scores = 49.96–128.41, $p = 0.001$–0.042), which was distributed over all ROIs throughout the M170 time window. Furthermore, there was a significant interaction between the category and SF (TFCE scores = 39.77–95.07, $p = 0.001$–0.027). This was driven by the spatiotemporal cluster consisting of a large number of data points (Fig. 2D).

3.4. Face-selectivity of M170 in the FG in each SF condition

The subsequent one-way ANOVA with the permutation test procedure and TFCE identified a significant difference between the category types in the BSF condition. This difference was driven by spatiotemporally distinct clusters (Table S2). Fig. 3A shows vertices included in one of the significant clusters, which was distributed over the lateral and medial FG from 151–183 ms (TFCE scores = 39.77–88.13, $p = 0.001$–0.027), and source waveforms at a representative vertex in the cluster. The included vertices vary depending on the time point (Fig. S6). Subsequent *post hoc* comparison using mean values within the cluster revealed significant differences between the face and house stimuli, with higher amplitudes for the face stimuli (Fig. 3B and Table 1). This indicates that the M170 component exhibits face-selectivity.

The one-way ANOVA also identified significant differences between the category types in the LSF and HSF conditions, with these differences driven by several spatiotemporal clusters within the significant interaction cluster (Table S2). Significant clusters with face-selectivity ranging over the lateral and medial FG were found in both SF conditions, but their time windows and included vertices were different (Table S5). A significant simple effect of category type was also observed in the IOG, and *post hoc* comparisons confirmed the presence of face-selectivity in these SF conditions (Table S5). Conversely, there was no significant difference in the EQU condition (TFCE scores = 0–36.22, $p \geq 0.077$).

Table 1
Results of *post hoc* paired comparisons for the effect of category in the BSF condition. Multiple comparisons were corrected by controlling the FDR. The significant simple effect clusters in the BSF condition had significantly higher values in the face conditions than in the house condition, indicating that the M170 is face-selective. The results in the medial FG further indicated the emotional effect of fear on the M170. The time windows in which vertices in each ROI showed significant simple effects are given in Table S3. The results from the LSF and HSF conditions are listed in Table S5. Note that we did not analyze single isolated vertices. Abbreviations: LatFG, lateral FG; MedFG, medial FG; IOG, inferior occipital gyrus; BSF, broadband spatial frequency; LSF, low spatial frequency; HSF, high spatial frequency. $^{*}p < 0.05$, $^{**}p < 0.01$, $^{***}p < 0.001$.

Region	Compared pair	*T* statistic	FDR-corrected *p* value
BSF (151–183 ms)			
Entire	Neutral vs. Fearful	51	0.133
	Neutral vs. House	5	**<0.001** ***
	Fearful vs. House	1	**<0.001** ***
LatFG	Neutral vs. Fearful	69	0.472
	Neutral vs. House	2	**<0.001** ***
	Fearful vs. House	3	**<0.001** ***
MedFG	Neutral vs. Fearful	35	**0.028** *
	Neutral vs. House	13	**0.002** **
	Fearful vs. House	1	**<0.001** ***

3.5. Emotional effect in the FG in the chromatic BSF condition

We conducted separate *post hoc* comparisons for the subclusters in individual ROIs to evaluate regional differences in the simple effects. Regarding the significant spatiotemporal cluster in the BSF condition at 151–183 ms, our analysis demonstrated that the spatiotemporal subclusters in both the lateral and medial FG showed face-selectivity, whereas only the subcluster in the medial FG showed significant differences between neutral and fearful faces (Fig. 3E and Table 1). This suggests that fearful emotion can influence the M170. In contrast, our analysis revealed no effect of emotion on the subclusters in the face-selective clusters in both the LSF and HSF conditions (Table S5).

3.6. Differential effects of SF on the ventral visual areas

One-way ANOVA identified a significant difference between the SF levels in the neutral face condition. This corresponded to a spatiotemporal cluster at 137–215 ms, which ranged across all ROIs (TFCE scores = 39.77–89.10, $p = 0.001$–0.027; Fig. 4A). *Post hoc* comparisons using mean values within the cluster revealed that the chromatic EQU stimuli elicited significantly smaller M170 responses compared with the other stimuli (Fig. 4B upper left and Table S6). Paired comparisons for subclusters in the lateral and medial FG further showed a significant difference between the chromatic BSF and LSF conditions (Fig. 4B upper middle and right), indicating that the LSF stimuli activated the FG significantly more than the BSF stimuli (Table S6). The IOG also showed a significantly larger response to the LSF and HSF stimuli compared with the BSF stimuli (Fig. 4B lower left and Table S6). V4 exhibited the same differences as those of the whole cluster, while no significant differences were found in V8 (Fig. 4B lower middle and right, and Table S6). Comparing data from the fearful face condition produced similar results (Table S6).

The time windows in which we observed significant spatiotemporal clusters corresponding to each simple effect are summarized in Fig. 5, and the effects revealed by *post hoc* comparisons are indicated by the colors of the rectangles. Distinct effects were found in different time windows, and the ranges of the time windows showing the same effects varied depending on the condition. The regions over which the significant spatiotemporal clusters extended were also unique (Tables S3 and S4).

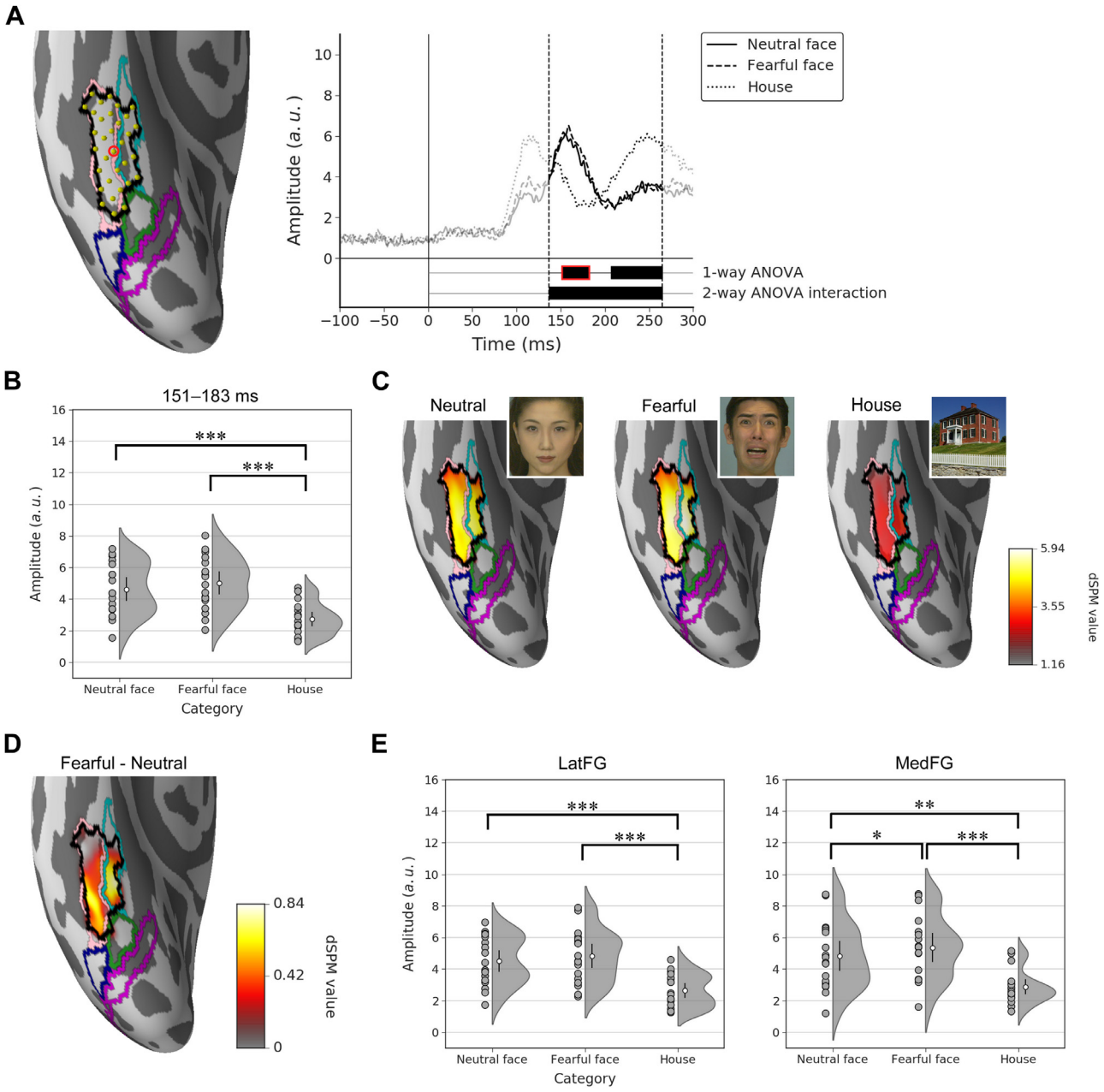

Fig. 3. Face-selectivity and emotional processing in the fusiform gyrus. **(A)** Significant spatiotemporal cluster for the effect of category in the BSF condition at 151–183 ms. The spatial extent of the cluster is indicated by a black line (left). The significant vertices (yellow spheres) were located in the lateral and medial FG (depicted by pink and cyan lines). Source waveforms at a representative vertex in the lateral FG (marked by a red circle in the left figure) are shown (right). The vertical line at 0 ms indicates stimulus onset. Black squares under the waveforms indicate the time windows in which we observed significant clusters for the simple effect of category by one-way ANOVA (upper) and significant clusters of the interaction by two-way ANOVA (lower). Both ANOVAs were performed using the permutation test procedure with TFCE. **(B)** Half-violin plots of mean dSPM values within a significant spatiotemporal cluster at 151–183 ms (red rectangle in A, right). Small circles on the left side indicate individual mean amplitudes within the cluster, and their distributions are depicted on the right side. White circles in the distributions indicate mean amplitudes across participants, and error bars represent 95% confidence intervals, which were estimated via a bootstrapping procedure with 5000 iterations. Face stimuli elicited components with larger amplitudes compared with house stimuli, indicating face-selectivity of the M170. **(C)** Spatial distributions of the mean dSPM values across participants and time points within the significant cluster at 151–183 ms for neutral (left) and fearful (middle) faces, and house images (right). The colored bar represents the magnitudes of the values. **(D)** Spatial distribution of the mean dSPM value differences between neutral and fearful face conditions. The colored bar represents the magnitude of the value difference, and larger values indicate that the region was activated more strongly in the fearful face condition. **(E)** Half-violin plots of mean dSPM values within subclusters in the lateral (left) and medial FG (right) at 151–183 ms. Fearful face stimuli elicited larger responses compared with neutral face stimuli within the significant cluster in the medial FG. Abbreviations: LatFG, lateral FG; MedFG, medial FG in this and Fig. 4. $^{*}p < 0.05$, $^{**}p < 0.01$, $^{***}p < 0.001$.

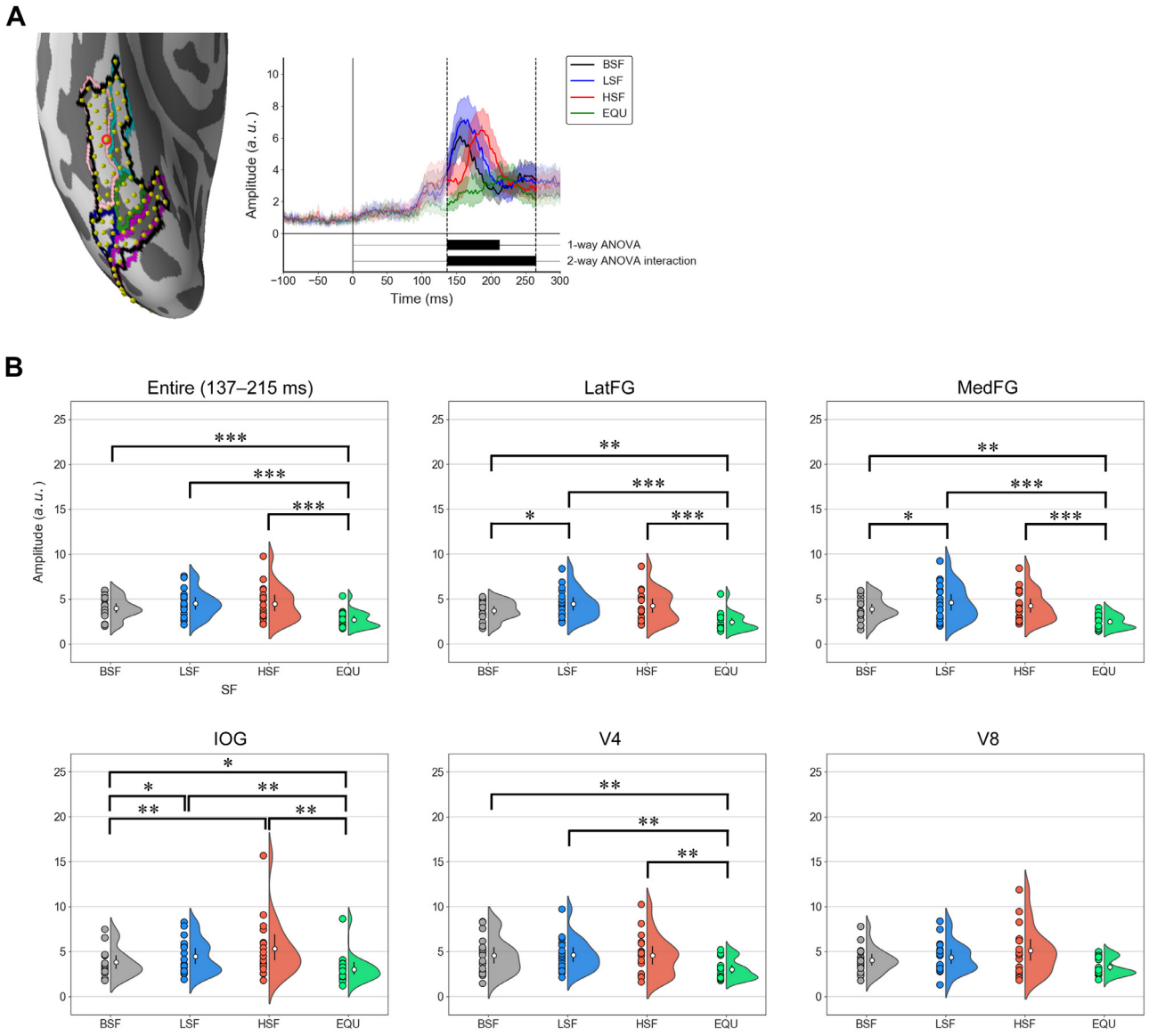

Fig. 4. Differential SF effects on each ROI. **(A)** Significant spatiotemporal cluster for the SF effect in the neutral face condition. Figures were made as in Fig. 3A. Note that the shading around the waveforms in the right figure represent 95% confidence intervals obtained via a bootstrapping procedure with 5000 iterations. The significant cluster ranged over all ROIs at 137–215 ms. **(B)** Mean dSPM values in the whole cluster at 137–215 ms (upper left) showed significant differences among EQU and the three SF conditions. The lateral (upper middle) and medial FG (upper right) also exhibited larger responses in the LSF than in the BSF condition. In addition, the HSF stimuli elicited a larger amplitude than the BSF stimuli in the IOG (lower left). V4 (lower middle) showed the same trend as that observed in the whole cluster, whereas no significant differences were observed for V8 (lower right). Figures were made as in Fig. 3B. $^{*}p < 0.05$, $^{**}p < 0.01$, $^{***}p < 0.001$.

3.7. Sequential processing of facial color information

Using the within-trial comparison approach together with the permutation test procedure with TFCE, we observed a significant activation above baseline elicited by the EQU neutral face stimuli. A significant cluster started at approximately 130 ms after stimulus onset (TFCE scores = 75.85–129.81, $p = 0.001$–0.004), within which activations were first observed around V4 and V8, followed by in FG (Fig. 6). We found a similar pattern in the fearful face condition, while the house stimuli seemed to elicit a different spatial distribution in the later time window (Fig. S7).

4. Discussion

Color and SF information from faces is conveyed via the M and P pathways and processed differently in the ventral visual stream. However, the ways in which color and SF information modulate neural activities in the human visual areas is largely unknown. In the present study, we manipulated broadband colored images of faces to create chromatic versions with different SF distributions but an equivalent mean luminance. To evaluate statistical significance with less arbitrariness, we adopted a statistical approach in which we combined a standard two-way ANOVA with a permutation test with TFCE. Our findings from the source-level analysis can be summarized as follows: In the BSF condition, M170 responses showed face-selectivity in the FG, and the M170 in the medial FG responded to fearful emotion. Although we also observed face-selectivity of the M170 in the FG and IOG in the LSF and HSF conditions, no emotional effect on M170 was observed. LSF face stimuli evoked a larger M170 response than BSF stimuli in the FG, while LSF and HSF stimuli elicited stronger IOG activation compared with BSF and EQU face stimuli. The smallest M170 amplitude was found in the EQU condition, with no significant differences among the category levels, al-

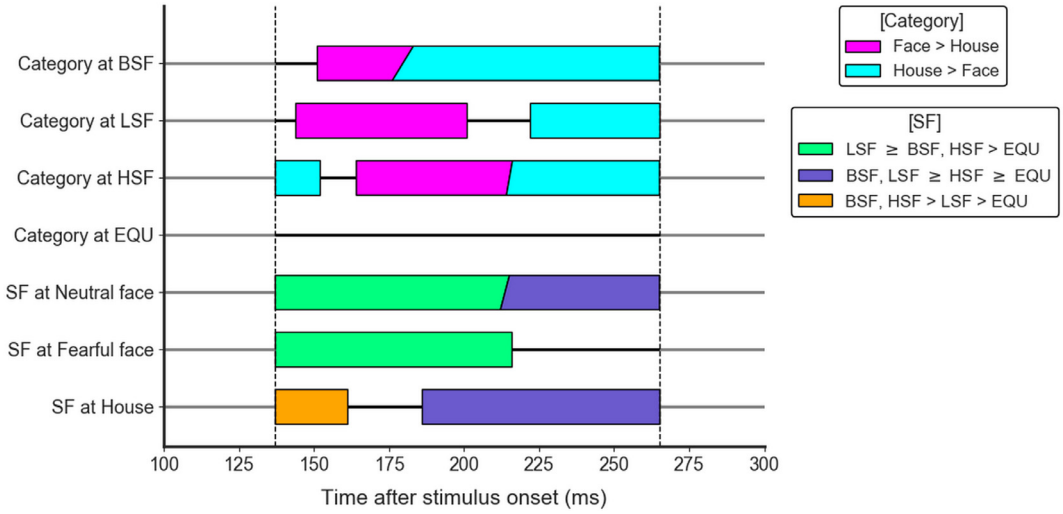

Fig. 5. Temporal profiles of significant spatiotemporal clusters of simple effects. Time windows of significant spatiotemporal clusters of simple effects are depicted by colored rectangles, and the colors indicate significant effects identified by *post hoc* paired comparisons. Vertical dashed lines represent the lower and upper limits of the M170 time window (137–265 ms). Some significant clusters were temporally overlapped, but spatially separated. Face-selectivity was found in the chromatic BSF, LSF, and HSF conditions but not in the EQU condition. Neutral and fearful face stimuli elicited similar neuromagnetic responses, whereas house stimuli elicited distinct SF effects.

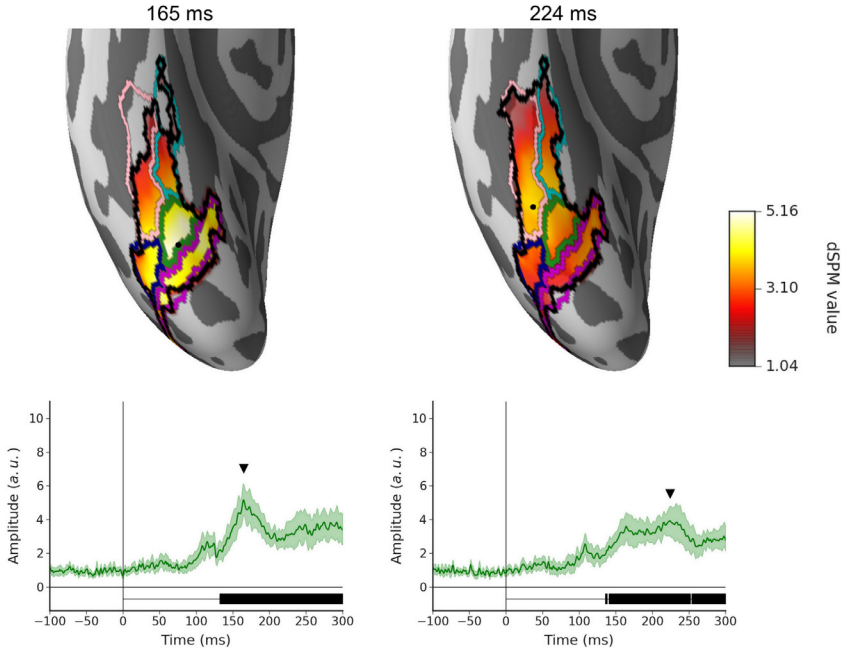

Fig. 6. Unique spatiotemporal profiles elicited by EQU face stimuli. Upper figures represent spatial distributions of mean dSPM values across participants in the EQU neutral face condition at 165 (left) and 224 ms (right). The colored bar represents the magnitudes of the mean values, and the black lines indicate the outer edges of clusters within ROIs. The peak of cortical activation at the early time point was located in V4 and V8, whereas the peak at the late time point was found in the lateral FG. Lower figures show source waveforms at representative vertices (black spheres in upper plots), and arrowheads indicate the time points at which the respective upper plots were obtained. The vertical line at 0 ms indicates the stimulus onset, and the shaded area around the waveforms represents 95% confidence intervals estimated via a bootstrapping procedure with 5000 iterations. The black shaded areas below the waveforms indicates the time windows in which amplitudes were significantly different from those in the pre-stimulus onset baseline period.

though a within-trial analysis revealed significant sequential activation of color-responsive regions and the FG.

4.1. Face-selectivity of the FG

The FG is considered to be the center of face perception (Haxby et al., 2000), and the M170 is thought to reflect FG activity (Deffke et al., 2007; Halgren et al., 2000; Perry and Singh, 2014; Pourtois et al., 2010). In accordance with this concept, we found that the M170 responses to face stimuli were significantly larger than those to house stimuli in the FG in all chromatic SF conditions, which indicates that the M170 has face-selectivity. In contrast, EQU chromatic stimuli, which have no specific SF components, did not elicit significantly different activation across categories. All three stimuli types contain SF components, and thus it is likely that the selective reactivity of the FG to faces is mainly derived from SF components. This interpretation is also supported by the results of numerous previous studies (Awasthi et al., 2013; Bentin et al., 1996; Deffke et al., 2007; Fan et al., 2020; Goffaux et al., 2003; Hsiao et al., 2005; Jeantet et al., 2019; Liu et al., 2000, 2002; McFadyen et al., 2017; Nakashima et al., 2008; Perry and Singh, 2014; Pourtois et al., 2010) that showed that grayscale face images elicited face-specific N170/M170 responses from the human brain.

4.2. Emotional processing in the medial FG

We found that chromatic BSF stimuli of fearful faces elicited a larger M170 response in the medial FG than those of neutral faces. It is well known that the amygdala, a subcortical structure located at the depth of the anterior temporal lobe, processes fearful emotion information

(Adolphs, 2002; LeDoux, 2000). Indeed, it is considered to be a node of the "extended system" of face processing (Haxby et al., 2000). MRI tractography studies have reported the existence of a white matter pathway linking the amygdala and FG (Rizzo et al., 2018; Smith et al., 2009), and a recent study using depth electrodes showed that the human amygdala responded to grayscale BSF and LSF fearful face stimuli faster than the FG (Méndez-Bértolo et al., 2016). Therefore, it is possible that the amygdala received and processed fear information from faces earlier than the FG and sent these signals to the FG via the white matter pathway, resulting in modified M170 responses in the FG. In addition, the previous findings that BSF and LSF stimuli elicited amygdala responses indicates that the M pathway projects to the amygdala from the retina (Méndez-Bértolo et al., 2016; Vuilleumier et al., 2003). Therefore, our finding that HSF fearful face stimuli did not elicit an emotional effect on M170 in the FG is consistent with previous work, and provides indirect support for the lack of amygdala contribution to the M170 when processing HSF stimuli.

We expected that the chromatic LSF fearful face stimuli, which was the preferred stimuli for the M system, could elicit large response in the FG as well (Méndez-Bértolo et al., 2016; Vuilleumier et al., 2003; Winston et al., 2003). However, we did not find such an effect in the LSF condition. Based on the observation that both the neutral and fearful faces in the LSF condition produced the largest mean values (Table S4), we speculate that the ceiling effect may have occurred in the FG. Namely, FG neurons may have been almost fully activated by the LSF stimuli. Consequently, additional processing of fear information from the amygdala in the FG may have been restricted by limited neuronal resources, leading to only slight modulation of M170 responses.

4.3. SF effect on the FG

The chromatic LSF face stimuli elicited larger M170 responses in the FG than the BSF stimuli. This result was unexpected because it meant that stimuli lacking physical features (HSF components) elicited larger FG activation than the original stimuli, which had intact SF distributions. Although previous fMRI studies have shown that the FG preferentially responds to LSF components (Canário et al., 2016; Woodhead et al., 2011), electrophysiological studies using grayscale LSF stimuli have been inconsistent regarding the magnitude of elicited N170/M170 amplitudes (Awasthi et al., 2013; Goffaux et al., 2003; Hsiao et al., 2005; Jeantet et al., 2019; McFadyen et al., 2017; Nakashima et al., 2008; Pourtois et al., 2010). To explain our unexpected results, we would like to introduce the following assumption: there exists an interaction between the M and P pathways during the processing of SF information in the FG. A previous study reported the potential existence of inhibitory interactions between the processes of different SF components in the neighboring PPA (Rajimehr et al., 2011). Assuming that the above-mentioned prerequisite is plausible, the interaction might disappear in the chromatic LSF face condition due to the lack of HSF components. This could have a disinhibition-like effect on LSF information processing, resulting in an increase in M170 responses in the FG to chromatic LSF stimuli. Interestingly, we found no significant differences between M170 amplitudes in the FG induced by chromatic HSF vs. BSF stimuli. Given that the FG has a response preference to LSF information (Canário et al., 2016; Woodhead et al., 2011), this disinhibition-like effect could be larger in the chromatic LSF than the HSF condition in the FG. To verify this assumption, further investigation is necessary.

4.4. Face-selectivity with the SF effect in the IOG

We found that, compared with house stimuli, chromatic LSF and HSF face stimuli evoked significant activation of the IOG (Table S5). The IOG contains a face-selective region called the occipital face area (OFA) (Gauthier et al., 2000) and is considered to process the local structural features of faces such as the mouth and eye (Liu et al., 2010; Pitcher et al., 2007). Previous studies have proposed a hierarchical model in which the IOG/OFA constitutes the "core system" of the face processing network where this region sends information about local face features to higher areas such as the FG (Haxby et al., 2000; Pitcher et al., 2011). Consistent with these notions, our results suggest that the IOG is face-selective. Moreover, in concordance with previous studies (Henson et al., 2009; Itier et al., 2006; Jacques et al., 2019; Rossion et al., 2003), our data indicate that the IOG contributes to the generation of M170 responses, because activation was observed in the M170 time window defined by the sensor ERF data.

To date, the relationship between SF face information and the face-selectivity of the IOG/OFA has not been well established. Several fMRI studies have suggested that these regions show preferential responses to HSF information in faces. For instance, Goffaux *et al.* reported that HSF face stimuli evoked larger activation of the OFA than HSF non-face control stimuli, while LSF face stimuli did not produce such activation (Goffaux et al., 2011). Further, using an adaptation paradigm, Rotshtein *et al.* found that the IOG strongly responded to the repetitive presentation of HSF face information (Rotshtein et al., 2007). In the present study, we observed significant face-selective IOG responses in both the LSF and HSF conditions. Our HSF data are in agreement with those of previous reports, but those regarding the LSF condition are not. This is probably because our LSF stimuli contained color information, which activated both the M and P pathways. Therefore, the increased IOG activity in the LSF condition could indicate that the IOG receives visual information from both pathways and that color information is important for face processing in the IOG.

By contrast, we did not observe face-selectivity of the IOG in the BSF condition. This may be related to our observation that the BSF and HSF house stimuli elicited larger neuromagnetic responses than the other SF stimuli in the early part of the M170 time window (Table S4). Because the time range of the SF effect in the house condition overlapped with the time window in which the M170 showed face-selectivity in the BSF condition (Fig. 5), a mixture of these activities may have occurred. In the HSF condition, the time window in which we found IOG face-selectivity was distinct (Fig. 5 and Table S4). This may explain why we could find face-selectivity.

We observed significantly larger IOG and FG activation in the LSF than in the BSF face condition (Table S6). This may indicate that an interaction between low and high SF, which we considered above, also exists in the IOG. However, unlike the FG, the IOG also showed significantly greater activation in the HSF than in the BSF condition, which may imply that the possible interaction of different SF processes is not biased in the IOG. Future studies are needed to clarify this issue.

4.5. Hierarchical processing of EQU face in the ventral face network

To date, the relationship between face color information and face processing is not fully understood. Psychophysical studies have shown that color information is beneficial for face recognition (Yip and Sinha, 2002), and more recently, that people can recognize emotion from face color information only, suggesting the importance of facial color for emotion perception (Benitez-Quiroz et al., 2018). Some electrophysiological studies compared M170 responses to chromatic and achromatic face stimuli, although their results were inconsistent. Schindler *et al.* recently observed that grayscale images elicited larger N170 amplitudes than color face stimuli (Schindler et al., 2019), while an earlier MEG work reported no significant difference between the responses to grayscale and color stimuli (Halgren et al., 2000). Our previous study using similar EQU stimuli (Nakashima et al., 2008) showed that grayscale BSF and chromatic face stimuli both elicited N170 responses, although the latencies of the components evoked by the chromatic images were prolonged (we obtained the same result in the sensor data analysis; see Supplementary Texts). Our detailed spatiotemporal mapping of ventral visual areas provides further insight regarding face color processing in the human brain.

Within-trial comparisons revealed that the FG was activated even when SF face information was fully removed. This result implies that, similar to SF information, color information could provide invariant face information related to face identity, which is thought to be processed by the FG (Haxby et al., 2000). A previous study also showed that face color can represent discriminable facial expressions of emotion (Benitez-Quiroz et al., 2018), indicating that face color can independently provide information regarding invariant and changeable aspects of faces, even in the absence of SF information. However, given that our ANOVA approach did not reveal statistically significant differences among categories, the intensity of the information provided by face color may not be as high as that of SF. Indeed, a previous psychophysical study reported that the contribution of color information to face recognition is supplementary (Yip and Sinha, 2002). This was evident when the shape information within face images was degraded by blurring.

We further observed that facial color information contained in the EQU face stimuli elicited neuromagnetic responses in color-responsive regions, V4 and V8, before activating the FG. A recent review (Grill-Spector et al., 2018) introduced a hierarchical face network model including the lower visual areas, and postulated that face information could be sent from V1 to the FG via V4. Although the authors did not detail the involvement of face color information in their network model, our results indicate that the proposed face processing network can process not only structural face information (SF component) but also face color information. Moreover, in good agreement with the hierarchical structure of this model, the sequential activation of V4/V8 and the FG suggest that facial color information is conveyed along the hierarchy of the ventral face network. Overall, our observations imply that SF-independent face processing by face color is plausible. Thus, a model of the face-processing network that considers the effect of face color information is needed.

4.6. Feasibility of SF-modulated chromatic stimuli

We developed a method for creating chromatic images in which SF information can be adjusted. Numerous studies have used grayscale stimuli with modulated SF components, whereas more complex chromatic stimuli, such as faces with modulated SF distributions, did not previously exist. The interchangeability between YCbCr and RGB color spaces prompted us to create spatially-filtered chromatic stimuli while preserving the color information and adjusting the mean luminance of the images. Creating EQU chromatic images similar to those used in a previous study (Nakashima et al., 2008) was also possible in a unified framework. In principle, this digital image processing technique is widely applicable to any type of natural RGB color picture, and could be a useful tool for future research. For instance, it may be useful for investigating the influence of SF and color in other category-selective visual areas.

Notably, the EQU images used in the present study were “theoretically equiluminant” but not “perceptually equiluminant.” Thus, the participants may have perceived the EQU stimuli differently, which may affect the face processing reflected in M170 responses. However, we used the “theoretically equiluminant” stimuli because (i) it was difficult to test individual equiluminant points between pairs of all colors contained in our stimuli and to modify them accordingly, and (ii) we wanted the visual inputs to all participants to be physically equivalent for comparisons with our previous study (Nakashima et al., 2008).

4.7. Mass univariate statistics with TFCE

MEG detects neuromagnetic activities on a millisecond scale and enables evaluation of activities at the brain surface with a fine spatial resolution using source reconstruction methods (Baillet, 2017; Hämäläinen et al., 1993; Hari and Puce, 2017; Tobimatsu and Kakigi, 2016). Assessing the statistical significance of individual data points in large spatiotemporal MEG datasets leads to the MCP because the data points are too numerous (Maris, 2012). Although researchers have developed various methodologies to avoid the MCP, these often yield other concerns. For example, while one frequently used approach involves adoption of common time windows and/or regions across conditions defined *a priori* (Keil et al., 2014), the range selection is subjective, and the data points within the ranges are frequently averaged. Cluster-based permutation testing (Maris and Oostenveld, 2007) is a more sophisticated approach, and is now a popular statistical procedure in EEG/MEG research because this method addresses the MCP successfully and does not require predefinitions. A recent study reported that this approach is more effective not only for exploratory research but also for evaluating well-known electrophysiological components (Fields and Kuperberg, 2020). However, cluster-based permutation testing requires an arbitrary threshold to form clusters, in addition to a significance level for statistical inference of the clusters (Maris and Oostenveld, 2007; Mensen and Khatami, 2013; Smith and Nichols, 2009) such that the choice of threshold can greatly affect the results.

The TFCE algorithm was first produced in the fMRI community (Smith and Nichols, 2009), and then introduced in EEG/MEG research (Mensen and Khatami, 2013; Pernet et al., 2015). A permutation test procedure with TFCE can successfully control the MCP as well as the cluster-based permutation test, and further resolve the aforementioned issues; the procedure dispenses with setting a threshold for cluster forming and predefining the data ranges (Mensen and Khatami, 2013; Smith and Nichols, 2009). Similar ANOVA approaches with TFCE have been used in previous EEG studies (Mensen et al., 2014, 2015, 2017), and the present study demonstrates that it is possible to solve a case in which a large number of data points show significant interactions by following a standard ANOVA procedure (Figs 2D and S4). Overall, this approach is considered more objective for assessing statistical significance. Thus, this procedure is expected to produce more reliable results (for further discussion, see Supplementary Texts).

4.8. Limitations

There are several limitations to the present study. First, we did not use grayscale images, and thus could not compare neural activities elicited by chromatic vs. achromatic stimuli. This was due to limits in the length of the experimental session to avoid participant fatigue. Second, our chromatic stimuli contained blue and yellow colors (Fig. 1A), and therefore we cannot exclude the possible influence of the koniocellular (K) pathway (Casagrande, 1994), which responds to blue-yellow color information. Given that the color information sent via the K pathway reaches V4 (Chang et al., 2014), it can affect processing in the ventral visual stream, although the functional role of the K pathway in the human brain remains uncertain. Third, as our stimuli had different color histograms between the SF conditions (Fig. S9), the color inputs into the P pathway are qualitatively different which may affect face processing. Fourth, although the present statistical procedure with TFCE enabled assessment of statistical significance without the restriction of data ranges, we defined the M170 time window statistically and adopted ROIs in the right hemisphere for computational efficiency. Moreover, our procedure cannot be used to assess statistical differences between ROIs because it checks the significance regardless of the regions in which the data points are included. For direct comparison between brain regions, a traditional method in which regions are set as a factor would be more useful.

5. Conclusion

The present study revealed the influences of parallel processing of SF and color on ventral visual areas, and indicated the presence of a complex relationship among visual pathways in the face processing system. We developed a technique for creating chromatic stimuli with adjusted

SF distributions and used a nonparametric statistical procedure with reduced arbitrariness. These methods are useful tools for examining the detailed spatiotemporal dynamics of face processing in humans and allowed us to determine the complex influences of different SF inputs with face color information on the M170.

CRediT author statement

Akinori Takeda: Conceptualization, Methodology, Software, Formal analysis, Investigation, Resources, Data Curation, Writing - Original Draft, Writing - Review & Editing, Visualization, Funding acquisition. **Emi Yamada:** Conceptualization, Methodology, Formal analysis, Investigation, Writing - Review & Editing, Funding acquisition. **Taira Uehara:** Methodology, Formal analysis, Writing - Review & Editing. **Katsuya Ogata:** Conceptualization, Methodology, Resources, Writing - Review & Editing. **Tsuyoshi Okamoto:** Methodology, Resources, Writing - Review & Editing. **Shozo Tobimatsu:** Conceptualization, Writing - Review & Editing, Supervision, Funding acquisition.

Data and code availability statement

The data acquired and analyzed in the present study cannot be made publicly available due to the absence of consent of the participants. Thus, the source data are only available from the corresponding author upon reasonable request for non-commercial academic purposes. Custom scripts are available on GitHub (https://github.com/AkinoriTakeda/M170_SFstudy).

Declaration of Competing Interest

None.

Acknowledgments

We thank Dr. Naruhito Hironaga for helpful advice regarding experimental design, and Dr. Hisato Nakazono for insightful comments regarding data analysis and interpretation. The present work was supported by Japan Society for the Promotion of Science (JSPS) KAKENHI Grant-in-Aid for JSPS Fellows [grant number JP18J11760] to A.T. and Grand-in-Aid for Early-Career Scientists [grant number JP18K15348] to E.Y. This work was also supported in part by Grant-in-Aid for Scientific Research on Innovative Areas MEXT KAKENHI [grant number JP15H05875] and Grant-in-Aid for Scientific Research (C) [grant number JP20K12573] to S.T. We thank Sydney Koke, MFA, from Edanz (https://jp.edanz.com) for editing a draft of this manuscript.

Supplementary materials

Supplementary material associated with this article can be found, in the online version, at doi:10.1016/j.neuroimage.2021.118325.

References

Adolphs, R., 2002. Neural systems for recognizing emotion. Curr. Opin. Neurobiol. 12, 169–177. doi:10.1016/S0959-4388(02)00301-X.

Amunts, K., Hawrylycz, M.J., Van Essen, D.C., Van Horn, J.D., Harel, N., Poline, J.B., De Martino, F., Bjaalie, J.G., Dehaene-Lambertz, G., Dehaene, S., Valdes-Sosa, P., Thirion, B., Zilles, K., Hill, S.L., Abrams, M.B., Tass, P.A., Vanduffel, W., Evans, A.C., Eickhoff, S.B., 2014. Interoperable atlases of the human brain. Neuroimage 99, 525–532. doi:10.1016/j.neuroimage.2014.06.010.

Awasthi, B., Sowman, P.F., Friedman, J., Williams, M.A., 2013. Distinct spatial scale sensitivities for early categorisation of faces and places: neuromagnetic and behavioural findings. Front. Human Neurosci. 7, 1–11. doi:10.3389/fnhum.2013.00091.

Baillet, S., 2017. Magnetoencephalography for brain electrophysiology and imaging. Nat. Neurosci. 20, 327–339. doi:10.1038/nn.4504.

Benitez-Quiroz, C.F., Srinivasan, R., Martinez, A.M., 2018. Facial color is an efficient mechanism to visually transmit emotion. PNAS 115, 3581–3586. doi:10.1073/pnas.1716084115.

Benjamini, Y., Hochberg, Y., 1995. Controlling the false discovery rate: a practical and powerful approach to multiple testing. J. R. Stat. Soc. 57, 289–300. doi:10.1111/j.2517-6161.1995.tb02031.x.

Bentin, S., Allison, T., Puce, A., Perez, E., McCarthy, G., 1996. Electrophysiological studies of face perception in humans. J. Cogn. Neurosci. 8, 551–565. doi:10.1162/jocn.1996.8.6.551.

Canário, N., Jorge, L., Loureiro Silva, M.F., Alberto Soares, M., Castelo-Branco, M., 2016. Distinct preference for spatial frequency content in ventral stream regions underlying the recognition of scenes, faces, bodies and other objects. Neuropsychologia 87, 110–119. doi:10.1016/j.neuropsychologia.2016.05.010.

Casagrande, V.A., 1994. A third parallel visual pathway to primate area V1. Trends Neurosci. 17, 305–310. doi:10.1016/0166-2236(94)90065-5.

Chang, M., Xian, S., Rubin, J., Moore, T., 2014. Latency of chromatic information in area V4. J. Physiol. Paris 108, 11–17. doi:10.1016/j.jphysparis.2013.05.006.

Cushing, C.A., Im, H.Y., Adams, R.B., Ward, N., Kveraga, K., 2019. Magnocellular and parvocellular pathway contributions to facial threat cue processing. Soc. Cognit. Affective Neurosci. 14, 151–162. doi:10.1093/scan/nsz003.

Dale, A.M., Liu, A.K., Fischl, B.R., Buckner, R.L., Belliveau, J.W., Lewine, J.D., Halgren, E., 2000. Dynamic statistical parametric mapping: combining fMRI and MEG for high-resolution imaging of cortical activity. Neuron 26, 55–67. doi:10.1016/S0896-6273(00)81138-1.

Deffke, I., Sander, T., Heidenreich, J., Sommer, W., Curio, G., Trahms, L., Lueschow, A., 2007. MEG/EEG sources of the 170-ms response to faces are co-localized in the fusiform gyrus. Neuroimage 35, 1495–1501. doi:10.1016/j.neuroimage.2007.01.034.

Eger, E., Schyns, P.G., Kleinschmidt, A., 2004. Scale invariant adaptation in fusiform face-responsive regions. Neuroimage 22, 232–242. doi:10.1016/j.neuroimage.2003.12.028.

Engemann, D.A., Gramfort, A., 2015. Automated model selection in covariance estimation and spatial whitening of MEG and EEG signals. Neuroimage 108, 328–342. doi:10.1016/j.neuroimage.2014.12.040.

Epstein, R., Kanwisher, N., 1998. A cortical representation of the local visual environment. Nature 392, 598–601. doi:10.1038/33402.

Evans, A.C., Janke, A.L., Collins, D.L., Baillet, S., 2012. Brain templates and atlases. Neuroimage 62, 911–922. doi:10.1016/j.neuroimage.2012.01.024.

Fan, X., Wang, F., Shao, H., Zhang, P., He, S., 2020. The bottom-up and top-down processing of faces in the human occipitotemporal cortex. eLife 9, 1–21. doi:10.7554/eLife.48764.

Fields, E.C., Kuperberg, G.R., 2020. Having your cake and eating it too: Flexibility and power with mass univariate statistics for ERP data. Psychophysiology 57, 1–21. doi:10.1111/psyp.13468.

Fischl, B., 2012. FreeSurfer. NeuroImage 62, 774–781. doi:10.1016/j.neuroimage.2012.01.021.

Gauthier, I., Tarr, M.J., Moylan, J., Skudlarski, P., Gore, J.C., Anderson, A.W., 2000. The fusiform “face area” is part of a network that processes faces at the individual level. J. Cogn. Neurosci. 12, 495–504. doi:10.1162/089892900562165.

Glasser, M.F., Coalson, T.S., Robinson, E.C., Hacker, C.D., Harwell, J., Yacoub, E., Ugurbil, K., Andersson, J., Beckmann, C.F., Jenkinson, M., Smith, S.M., Van Essen, D.C., 2016. A multi-modal parcellation of human cerebral cortex. Nature 536, 171–178. doi:10.1038/nature18933.

Goffaux, V., Gauthier, I., Rossion, B., 2003. Spatial scale contribution to early visual differences between face and object processing. Cognitive Brain Res. 16, 416–424. doi:10.1016/S0926-6410(03)00056-9.

Goffaux, V., Peters, J., Haubrechts, J., Schiltz, C., Jansma, B., Goebel, R., 2011. From coarse to fine? spatial and temporal dynamics of cortical face processing. Cereb. Cortex 21, 467–476. doi:10.1093/cercor/bhq112.

Gramfort, A., Luessi, M., Larson, E., Engemann, D.A., Strohmeier, D., Brodbeck, C., Goj, R., Jas, M., Brooks, T., Parkkonen, L., Hämäläinen, M., 2013. MEG and EEG data analysis with MNE-Python. Front. Neurosci. 7, 1–13. doi:10.3389/fnins.2013.00267.

Gramfort, A., Luessi, M., Larson, E., Engemann, D.A., Strohmeier, D., Brodbeck, C., Parkkonen, L., Hämäläinen, M.S., 2014. MNE software for processing MEG and EEG data. Neuroimage 86, 446–460. doi:10.1016/j.neuroimage.2013.10.027.

Grill-Spector, K., Weiner, K.S., Gomez, J., Stigliani, A., Natu, V.S., 2018. The functional neuroanatomy of face perception: From brain measurements to deep neural networks. Interface Focus 8. doi:10.1098/rsfs.2018.0013.

Hadjikhani, N., Liu, A.K., Dale, A.M., Cavanagh, P., Tootell, R.B.H., 1998. Retinotopy and color sensitivity in human visual cortical area V8. Nat. Neurosci. 1, 235–241. doi:10.1038/681.

Halgren, E., Raij, T., Marinkovic, K., Jousmäki, V., Hari, R., 2000. Cognitive response profile of the human fusiform face area as determined by MEG. Cereb. Cortex 10, 69–81. doi:10.1093/cercor/10.1.69.

Hämäläinen, M., Hari, R., Ilmoniemi, R.J., Knuutila, J., Lounasmaa, O.V., 1993. Magnetoencephalography - theory, instrumentation, and applications to noninvasive studies of the working human brain. Rev. Mod. Phys. 65, 413–497. doi:10.1103/RevModPhys.65.413.

Hari, R., Puce, A., 2017. MEG-EEG Primer. Oxford University Press doi:10.1093/med/9780190497774.001.0001.

Haxby, J.V, Hoffman, E.A., Gobbini, M.I., 2000. The distributed human neural system for face perception. Trends Cogn. Sci. 4, 223–233. doi:10.1016/S1364-6613(00)01482-0.

Henson, R.N., Mouchlianitis, E., Friston, K.J., 2009. MEG and EEG data fusion: simultaneous localisation of face-evoked responses. Neuroimage 47, 581–589. doi:10.1016/j.neuroimage.2009.04.063.

Hsiao, F.J., Hsieh, J.C., Lin, Y.Y., Chang, Y., 2005. The effects of face spatial frequencies on cortical processing revealed by magnetoencephalography. Neurosci. Lett. 380, 54–59. doi:10.1016/j.neulet.2005.01.016.

Iidaka, T., Yamashita, K., Kashikura, K., Yonekura, Y., 2004. Spatial frequency of visual image modulates neural responses in the temporo-occipital lobe. An investigation with event-related fMRI. Cognitive Brain Res. 18, 196–204. doi:10.1016/j.cogbrainres.2003.10.005.

Im, H.Y., Adams, R.B., Boshyan, J., Ward, N., Cushing, C.A., Kveraga, K., 2017. Observer's anxiety facilitates magnocellular processing of clear facial threat cues, but impairs parvocellular processing of ambiguous facial threat cues. Sci. Rep. 7, 1–13. doi:10.1038/s41598-017-15495-2.

Itier, R.J., Herdman, A.T., George, N., Cheyne, D., Taylor, M.J., 2006. Inversion and contrast-reversal effects on face processing assessed by MEG. Brain Res. 1115, 108–120. doi:10.1016/j.brainres.2006.07.072.

Jacques, C., Jonas, J., Maillard, L., Colnat-Coulbois, S., Koessler, L., Rossion, B., 2019. The inferior occipital gyrus is a major cortical source of the face-evoked N170: Evidence from simultaneous scalp and intracerebral human recordings. Hum. Brain Mapp. 40, 1403–1418. doi:10.1002/hbm.24455.

Jas, M., Larson, E., Engemann, D.A., Leppäkangas, J., Taulu, S., Hämäläinen, M., Gramfort, A., 2018. A reproducible MEG/EEG group study with the MNE software: recommendations, quality assessments, and good practices. Front. Neurosci. 12, 1–18. doi:10.3389/fnins.2018.00530.

Jeantet, C., Caharel, S., Schwan, R., Lighezzolo-Alnot, J., Laprevote, V., 2018. Factors influencing spatial frequency extraction in faces: a review. Neurosci. Biobehav. Rev. 93, 123–138. doi:10.1016/j.neubiorev.2018.03.006.

Jeantet, C., Laprevote, V., Schwan, R., Schwitzer, T., Maillard, L., Lighezzolo-Alnot, J., Caharel, S., 2019. Time course of spatial frequency integration in face perception: an ERP study. Int. J. Psychophysiol. 143, 105–115. doi:10.1016/j.ijpsycho.2019.07.001.

Kanwisher, N., McDermott, J., Chun, M.M., 1997. The fusiform face area: a module in human extrastriate cortex specialized for face perception. J. Neurosci. 17, 4302–4311. doi:10.1523/JNEUROSCI.17-11-04302.1997.

Keil, A., Debener, S., Gratton, G., Junghöfer, M., Kappenman, E.S., Luck, S.J., Luu, P., Miller, G.A., Yee, C.M., 2014. Committee report: publication guidelines and recommendations for studies using electroencephalography and magnetoencephalography. Psychophysiology 51, 1–21. doi:10.1111/psyp.12147.

Lang, P.J., Bradley, M.M., Cuthbert, B.N., 2008. International Affective Picture System (IAPS): Affective Ratings of Pictures and Instruction Manual. University of Florida, Gainesville, FL Technical Report A-8.

Larson, E., Taulu, S., 2018. Reducing sensor noise in MEG and EEG recordings using oversampled temporal projection. IEEE Trans. Biomed. Eng. 65, 1002–1013. doi:10.1109/TBME.2017.2734641.

LeDoux, J.E., 2000. Emotion circuits in the brain. Annu. Rev. Neurosci. 23, 155–184. doi:10.1146/annurev.neuro.23.1.155.

Liu, J., Harris, A., Kanwisher, N., 2010. Perception of face parts and face configurations: an fMRI study. J. Cogn. Neurosci. 22, 203–211. doi:10.1162/jocn.2009.21203.

Liu, J., Harris, A., Kanwisher, N., 2002. Stages of processing in face perception: an MEG study. Nat. Neurosci. 5, 910–916. doi:10.1038/nn909.

Liu, J., Higuchi, M., Marantz, A., Kanwisher, N., 2000. The selectivity of the occipitotemporal M170 for faces. Neuroreport 11, 337–341. doi:10.1097/00001756-200002070-00023.

Livingstone, M., Hubel, D., 1988. Segregation of form, color, movement, and depth: anatomy, physiology, and perception. Science 240, 740–749. doi:10.1126/science.3283936.

Maris, E., 2012. Statistical testing in electrophysiological studies. Psychophysiology 49, 549–565. doi:10.1111/j.1469-8986.2011.01320.x.

Maris, E., Oostenveld, R., 2007. Nonparametric statistical testing of EEG- and MEG-data. J. Neurosci. Methods 164, 177–190. doi:10.1016/j.jneumeth.2007.03.024.

McFadyen, J., Mermillod, M., Mattingley, J.B., Halász, V., Garrido, M.I., 2017. A rapid subcortical amygdala route for faces irrespective of spatial frequency and emotion. J. Neurosci. 37, 3864–3874. doi:10.1523/JNEUROSCI.3525-16.2017.

McKeefry, D.J., Zeki, S., 1997. The position and topography of the human colour centre as revealed by functional magnetic resonance imaging. Brain 120, 2229–2242. doi:10.1093/brain/120.12.2229.

Méndez-Bértolo, C., Moratti, S., Toledano, R., Lopez-Sosa, F., Martínez-Alvarez, R., Mah, Y.H., Vuilleumier, P., Gil-Nagel, A., Strange, B.A., 2016. A fast pathway for fear in human amygdala. Nat. Neurosci. 19, 1041–1049. doi:10.1038/nn.4324.

Mensen, A., Khatami, R., 2013. Advanced EEG analysis using threshold-free cluster-enhancement and non-parametric statistics. Neuroimage 67, 111–118. doi:10.1016/j.neuroimage.2012.10.027.

Mensen, A., Marshall, W., Tononi, G., 2017. EEG differentiation analysis and stimulus set meaningfulness. Front. Psychol. 8, 1748. doi:10.3389/fpsyg.2017.01748.

Mensen, A., Poryazova, R., Huegli, G., Baumann, C.R., Schwartz, S., Khatami, R., 2015. The roles of dopamine and hypocretin in reward: a electroencephalographic study. PLoS One 10, 1–15. doi:10.1371/journal.pone.0142432.

Mensen, A., Poryazova, R., Schwartz, S., Khatami, R., 2014. Humor as a reward mechanism: Event-related potentials in the healthy and diseased brain. PLoS One 9. doi:10.1371/journal.pone.0085978.

Merigan, W.H., Maunsell, J.H.R., 1993. How parallel are the primate visual pathways. Annu. Rev. Neurosci. 16, 369–402. doi:10.1146/annurev.neuro.16.1.369.

Morrison, D.J., Schyns, P.G., 2001. Usage of spatial scales for the categorization of faces, objects, and scenes. Psychon. Bull. Rev. 8, 454–469. doi:10.3758/BF03196180.

Nakashima, T., Kaneko, K., Goto, Y., Abe, T., Mitsudo, T., Ogata, K., Makinouchi, A., Tobimatsu, S., 2008. Early ERP components differentially extract facial features: Evidence for spatial frequency-and-contrast detectors. Neurosci. Res. 62, 225–235. doi:10.1016/j.neures.2008.08.009.

Oldfield, R.C., 1971. The assessment and analysis of handedness: the Edinburgh inventory. Neuropsychologia 9, 97–113. doi:10.1016/0028-3932(71)90067-4.

Peirce, J., Gray, J.R., Simpson, S., MacAskill, M., Höchenberger, R., Sogo, H., Kastman, E., Lindeløv, J.K., 2019. PsychoPy2: Experiments in behavior made easy. Behav. Res. Methods 51, 195–203. doi:10.3758/s13428-018-01193-y.

Peirce, J.W., 2007. PsychoPy-psychophysics software in python. J. Neurosci. Methods 162, 8–13. doi:10.1016/j.jneumeth.2006.11.017.

Pernet, C.R., Latinus, M., Nichols, T.E., Rousselet, G.A., 2015. Cluster-based computational methods for mass univariate analyses of event-related brain potentials/fields: a simulation study. J. Neurosci. Methods 250, 85–93. doi:10.1016/j.jneumeth.2014.08.003.

Perry, G., Singh, K.D., 2014. Localizing evoked and induced responses to faces using magnetoencephalography. Eur. J. Neurosci. 39, 1517–1527. doi:10.1111/ejn.12520.

Pitcher, D., Walsh, V., Duchaine, B., 2011. The role of the occipital face area in the cortical face perception network. Exp. Brain Res. 209, 481–493. doi:10.1007/s00221-011-2579-1.

Pitcher, D., Walsh, V., Yovel, G., Duchaine, B., 2007. TMS evidence for the involvement of the right occipital face area in early face processing. Curr. Biol. 17, 1568–1573. doi:10.1016/j.cub.2007.07.063.

Pourtois, G., Spinelli, L., Seeck, M., Vuilleumier, P., 2010. Modulation of face processing by emotional expression and gaze direction during intracranial recordings in right fusiform cortex. J. Cogn. Neurosci. 22, 2086–2107. doi:10.1162/jocn.2009.21404.

Prieto, E.A., Caharel, S., Henson, R., Rossion, B., 2011. Early (N170/M170) face-sensitivity despite right lateral occipital brain damage in acquired prosopagnosia. Front. Human Neurosci. 5, 1–23. doi:10.3389/fnhum.2011.00138.

Rajimehr, R., Devaney, K.J., Bilenko, N.Y., Young, J.C., Tootell, R.B.H., 2011. The "parahippocampal place area" responds preferentially to high spatial frequencies in humans and monkeys. PLoS Biol. 9. doi:10.1371/journal.pbio.1000608.

Rizzo, G., Milardi, D., Bertino, S., Basile, G.A., Di Mauro, D., Calamuneri, A., Chillemi, G., Silvestri, G., Anastasi, G., Bramanti, A., Cacciola, A., 2018. The limbic and sensorimotor pathways of the human amygdala: a structural connectivity study. Neuroscience 385, 166–180. doi:10.1016/j.neuroscience.2018.05.051.

Rossion, B., Joyce, C.A., Cottrell, G.W., Tarr, M.J., 2003. Early lateralization and orientation tuning for face, word, and object processing in the visual cortex. Neuroimage 20, 1609–1624. doi:10.1016/j.neuroimage.2003.07.010.

Rotshtein, P., Schofield, A., Funes, M.J., Humphreys, G.W., 2010. Effects of spatial frequency bands on perceptual decision: It is not the stimuli but the comparison. Journal of Vision 10, 1–20. doi:10.1167/10.10.25.

Rotshtein, P., Vuilleumier, P., Winston, J., Driver, J., Dolan, R., 2007. Distinct and convergent visual processing of high and low spatial frequency information in faces. Cereb. Cortex 17, 2713–2724. doi:10.1093/cercor/bhl180.

Schindler, S., Bruchmann, M., Bublatzky, F., Straube, T., 2019. Modulation of face- and emotion-selective ERPs by the three most common types of face image manipulations. Social Cogn. Affective Neurosci. 14, 493–503. doi:10.1093/scan/nsz027.

Skottun, B.C., 2000. The magnocellular deficit theory of dyslexia: the evidence from contrast sensitivity. Vision Res. 40, 111–127. doi:10.1016/S0042-6989(99)00170-4.

Smith, C.D., Lori, N.F., Akbudak, E., Sorar, E., Gultepe, E., Shimony, J.S., McKinstry, R.C., Conturo, T.E., 2009. MRI diffusion tensor tracking of a new amygdalo-fusiform and hippocampo-fusiform pathway system in humans. J. Magn. Reson. Imaging 29, 1248–1261. doi:10.1002/jmri.21692.

Smith, S.M., Nichols, T.E., 2009. Threshold-free cluster enhancement: addressing problems of smoothing, threshold dependence and localisation in cluster inference. Neuroimage 44, 83–98. doi:10.1016/j.neuroimage.2008.03.061.

Stenroos, M., Hunold, A., Haueisen, J., 2014. Comparison of three-shell and simplified volume conductor models in magnetoencephalography. Neuroimage 94, 337–348. doi:10.1016/j.neuroimage.2014.01.006.

Taulu, S., Simola, J., 2006. Spatiotemporal signal space separation method for rejecting nearby interference in MEG measurements. Phys. Med. Biol. 51, 1759–1768. doi:10.1088/0031-9155/51/7/008.

Tobimatsu, S., Celesia, G.G., 2006. Studies of human visual pathophysiology with visual evoked potentials. Clin. Neurophysiol. 117, 1414–1433. doi:10.1016/j.clinph.2006.01.004.

Tobimatsu, S., Kakigi, R., 2016. Clinical Applications of Magnetoencephalography. Springer, Japan, Tokyo doi:10.1007/978-4-431-55729-6.

Vuilleumier, P., Armony, J.L., Driver, J., Dolan, R.J., 2003. Distinct spatial frequency sensitivities for processing faces and emotional expressions. Nat. Neurosci. 6, 624–631. doi:10.1038/nn1057.

Weiner, K.S., Grill-Spector, K., 2010. Sparsely-distributed organization of face and limb activations in human ventral temporal cortex. Neuroimage 52, 1559–1573. doi:10.1016/j.neuroimage.2010.04.262.

Willenbockel, V., Sadr, J., Fiset, D., Horne, G.O., Gosselin, F., Tanaka, J.W., 2010. Controlling low-level image properties: The SHINE toolbox. Behav. Res. Methods 42, 671–684. doi:10.3758/BRM.42.3.671.

Winston, J.S., Vuilleumier, P., Dolan, R.J., 2003. Effects of low-spatial frequency components of fearful faces on fusiform cortex activity. Curr. Biol. 13, 1824–1829. doi:10.1016/j.cub.2003.09.038.

Woodhead, Z.V.J., Wise, R.J.S., Sereno, M., Leech, R., 2011. Dissociation of sensitivity to spatial frequency in word and face preferential areas of the fusiform gyrus. Cereb. Cortex 21, 2307–2312. doi:10.1093/cercor/bhr008.

Yip, A.W., Sinha, P., 2002. Contribution of color to face recognition. Perception 31, 995–1003. doi:10.1068/p3376.